HHS Public Access

Author manuscript

Int J Radiat Oncol Biol Phys. Author manuscript; available in PMC 2022 January 13.

Published in final edited form as:

Int J Radiat Oncol Biol Phys. 2020 November 01; 108(3): 745–757. doi:10.1016/j.ijrobp.2020.05.027.

Neuroinflammation After Stereotactic Radiosurgery-Induced Brain Tumor Disintegration Is Linked to Persistent Cognitive Decline in a Mouse Model of Metastatic Disease

Chengyan Chu, MD[*,†], **Catherine M. Davis, PhD**[‡], **Xiaoyan Lan, MD**[*,†], **Robert D. Hienz, PhD**[‡], **Anna Jablonska, PhD**[*,†], **Aline M. Thomas, PhD**[†], **Esteban Velarde, BSc**[§], **Shen Li, MD, PhD**[‖], **Miroslaw Janowski, MD, PhD**[*,†], **Mihoko Kai, PhD**[§], **Piotr Walczak, MD, PhD**[*,†]

[*]Department of Diagnostic Radiology and Nuclear Medicine, University of Maryland School of Medicine, Baltimore, Maryland;

[†]The Russell H. Morgan Department of Radiology and Radiological Science, Johns Hopkins University School of Medicine, Baltimore, Maryland;

[‡]Division of Behavioral Biology, Department of Psychiatry and Behavioral Sciences, Johns Hopkins University School of Medicine, Baltimore, Maryland;

[§]Department of Radiation Oncology, Johns Hopkins University, School of Medicine, Baltimore, Maryland;

[‖]Department of Neurology, Dalian Municipal Central Hospital, Dalian, Liaoning, China

Abstract

Purpose: Improved efficacy of anticancer therapy and a growing pool of survivors give rise to a question about their quality of life and return to premorbid status. Radiation is effective in brain metastasis eradication, although the optimal approach and long-term effects on brain function are largely unknown. We studied the effects of radiosurgery on brain function.

Methods and Materials: Adult C57BL/6J mice with or without brain metastases (rat 9L gliosarcoma) were treated with cone beam single-arc stereotactic radiosurgery (SRS; 40 Gy). Tumor growth was monitored using bioluminescence, whereas longitudinal magnetic resonance imaging, behavioral studies, and histologic analysis were performed to evaluate brain response to the treatment for up to 18 months.

Results: Stereotactic radiosurgery (SRS) resulted in 9L metastases eradication within 4 weeks with subsequent long-term survival of all treated animals, whereas all nontreated animals succumbed to the brain tumor. Behavioral impairment, as measured with a recognition memory test, was observed earlier in mice subjected to radiosurgery of tumors (6 weeks) in comparison to SRS of healthy brain tissue (10 weeks). Notably, the deficit resolved by 18 weeks only in mice not bearing a tumor, whereas tumor eradication was complicated by the persistent cognitive

Corresponding authors: Mihoko Kai, PhD; mkai2@jhmi.edu or Piotr Walczak, MD, PhD; pwalczak@som.umaryland.edu.

Disclosures: The authors declare no conflict of interest related to this study.

All data generated and analyzed during this study are included in this published article (and its supplementary information files).

Supplementary material for this article can be found at https://doi.org/10.1016/j.ijrobp.2020.05.027.

deficits. In addition, the results of magnetic resonance imaging were unremarkable in both groups, and histopathology revealed changes. SRS-induced tumor eradication triggered long-lasting and exacerbated neuroinflammatory response. No demyelination, neuronal loss, or hemorrhage was detected in any of the groups.

Conclusions: Tumor disintegration by SRS leads to exacerbated neuroinflammation and persistent cognitive deficits; therefore, methods aiming at reducing inflammation after tumor eradication or other therapeutic methods should be sought.

Summary

Cancer treatment is becoming more effective with a growing number of long-term survivors. Therefore, the quality of life after treatment is becoming an increasingly important aspect. Brain metastases have been traditionally a major problem, but radiation-based approaches frequently lead to their cure, though there is no agreement regarding optimal approach. There is also a scarcity of data on long-term effects of therapy on brain function. Here, we studied long-term outcomes of radiosurgery-based eradication of brain metastases and compared its effects of radiosurgical dose of radiation on a healthy brain in the mouse model. We also focused on the cognitive aspect of behavior to specifically address the clinical problem. Notably, we found that radiosurgery had only transient effect on cognition in naive animals, while irradiation of brain tumors led to more severe neuroinflammation and permanent cognitive deficits. We conclude that more attention is needed to combat the consequences of neuroinflammation after eradicating brain metastases.

Introduction

Cancer treatment is frequently associated with a persistent cognitive decline, and “chemobrain” is a well-recognized sequela of chemotherapeutic agent administration.[1] Brain metastases are the most common intracranial malignancy, occurring in an estimated 20% of all patients with cancer.[2] The incidence of brain metastases even increased as systemic therapies became more effective, and patients at the stage of metastatic disease are living longer.[3] The advanced FLASH radiation therapy based on ultrafast delivery of radiation treatment at dose rates several orders of magnitude greater than those currently in routine clinical practice has shown remarkable normal tissue sparing compared with the conventional dose rate, thereby preserving neurocognitive function.[4] However, this attractive technology is not yet widely available and still needs more development before routine clinical implementation. Currently, stereotactic radiosurgery (SRS) has been shown to be effective in eradication of brain metastasis, although its effect on a patient’s cognitive decline has been rarely studied.[5] As the rate at which cancer is cured is improving, there is an urgent need to obtain more insight into cognitive function and quality of life of long-term survivors subjected to SRS, to seek solutions to prevent cognitive decline, as precipitating numbers of disabled cancer survivors is a serious concern.

The effect of brain metastasis SRS on cognitive function is rarely studied in the preclinical setting, and clinical outcomes are ambiguous. Here, we studied consequences of SRS of brain metastases on brain function and neuropathology, taking advantage of custom-built small animal radiation research platform for precision focal irradiation.[6] Tumor

growth and eradication were monitored with bioluminescence imaging. Brain response to therapy has been characterized by a comprehensive set of readouts: MRI, behavior, and postmortem tissue analysis. Because cognitive decline is a most frequent complaint of cancer survivors, we selected behavioral tests aimed at addressing this domain. We chose 9L rat gliosarcoma as a tumor model because of its non-infiltrative growth pattern resembling brain metastasis.[7,8] The selection of a 40-Gy dose stemmed from previous failures of 9L eradication by lower doses of radiation including 20 and 25 Gy.[9,10] Our advances in induction of transient tolerance to brain cancer xenografts based on blocking costimulation signaling with monoclonal antibodies allowed us to take advantage of mouse as a versatile recipient.[11] Importantly, blocking antibodies were only injected after tumor cell implantation, and they completely clear within weeks,[11–13] leaving the immune system fully intact.

Materials and Methods

Cell culture and lentiviral transduction

Rat 9L glioma cells (American Type Culture Collection) were transduced with a lentiviral construct containing fluorescent and luciferase reporter genes under the constitutive promoter. Lentivirus was generated as we described previously[14] and applied to 9L glioma cells for 48 hours.[15] The luciferase expression of transduced cells was measured using Xenogen IVIS optical imaging system and Living Image software (Perkin Elmer). The fluorescence *mCherry* reporter signal was observed using an inverted microscope (Zeiss, Axio Observer Z1). Next, 9L cells highly expressing the reporter were expanded in RPMI 1640 Medium (ThermoFisher Scientific) containing 10% fetal bovine serum (FBS, Gibco) and 1% penicillin/streptomycin (Sigma) and then prepared for transplantation.

Tumor implantation

All procedures involving live animals complied with the ARRIVE guidelines and were approved and performed in accordance with the National Institutes of Health Guide for the Care and Use of Laboratory Animals.[16] Thirty-seven male C57BL/6J mice (6–8 weeks old, 20–25 g; Jackson Laboratory) were used in the study. Animals were divided into 4 experimental groups: tumor-free mice (sham; n = 3), tumor-free mice with ionizing irradiation (sham + SRS; n = 14), tumor-bearing mice without SRS (tumor; n = 8), and tumor-bearing mice with irradiation (tumor + SRS; n = 14). For tumor implantation, animals were anesthetized with isoflurane: 4% for induction and 1.5% to 2% for maintenance. After positioning in a stereotaxic frame, the burr hole was placed at the following coordinates: anteroposterior = 0.5 mm; mediolateral = 2.0 mm; dorsoventral = 2.5 mm. Then, 2×10^5 cells suspended in 2 μL phosphate-buffered saline (PBS) were injected into striatum at a rate of 0.5 μL/min using a 31-gauge microneedle attached to a 10-μL Hamilton syringe. The needle was kept in place for 5 minutes after completion of the injection to prevent backflow. To induce tolerance to tumors, animals were administered with Hamster antimouse-CD154mAb (MR1, BioXcell; Lebanon, NH) and CTLA4-Ig (Bristol-Myers Squibb, Princeton, NJ) (500 μg/each, intraperitoneally) on days 0, 2, 4 and 6 as described previously.[11] Tumor-free mice (referred to as *Sham*) also underwent the same surgical procedures, except that they were injected with PBS only.

SRS

Nine days after surgery, animals in the sham + SRS and tumor + SRS groups received a single arc radiation exposure of 40 Gy. The mice were anesthetized with 2% isoflurane and placed in prone position on the treatment table and irradiated using a custom-built small animal radiation research platform, equipped with on-board computed tomographic (CT) guidance to facilitate precise targeting during radiation therapy. After 3-dimensional CT image acquisition, a target spot with the iso-center was located according to the drilling hole in the skull and 2.5 mm deep relative to the hole, the same depth as tumor and PBS injection (Fig. 1A). Next, the target spot was irradiated with a single beam (angle = 60°), using a 5 × 5-mm^2 collimator at a dose of 40 Gy. Notably, as shown in Fig. 1B, the radiation targeted on the outlined area intentionally avoided the hippocampus not to directly compromise the hippocampal neurogenesis.

Bioluminescence imaging

Bioluminescence imaging (BLI) was used to monitor tumor growth rate and was initiated 1 day after tumor implantation. Animals were anesthetized with 2% isoflurane and injected intraperitoneally with 150 μL luciferin (15 mg/mL). Images were acquired 5 to 15 minutes after injection at the peak of the bioluminescence signal. For BLI analysis, images were quantified by drawing regions of interest. The data were expressed as photon flux (P/sec) and plotted using GraphPad Prism 8.

Magnetic resonance imaging

Magnetic resonance imaging (MRI) was performed under general anesthesia (1.5%–2.0 % isoflurane) to visualize brain tissue response to tumor and to irradiation. The 11.7-T Bruker Biospec system (Bruker, Ettlingen, Germany) and a surface coil array were used for image acquisition. T2-weighted images (T2WI) were obtained using a Rapid Imaging with Refocused Echoes (RARE) sequence with the following parameters: echo time (TE) = 30 ms; repetition time (TR) = 2500 ms; slice thickness (ST) = 0.7 mm; average (AV) = 2; FOV = 14 × 14 mm^2; matrix size = 256 × 256; and Rapid Imaging with Refocused Echoes factor = 8. To visualize bloodebrain barrier (BBB) integrity, T1-weighted images (T1WI) were acquired (TE = 7 ms, TR = 350 ms, AV = 2) before and 5 minutes after gadolinium administration (70 μL; 1 mmol/mL, intraperitoneally) with the same geometry and location as the T2WI. National Institutes of Health ImageJ software was used for image analysis. The tumor and the brain were delineated manually on the T2WI, and the volumes were calculated from a series of slices. Irradiated (ipsilateral) and contralateral hemispheres in T1WI-gadolinium images were followed separately; the pixel intensity was measured to report on BBB permeability.

Behavior assessment

Social odor-recognition memory test—The social odor-recognition memory (SORM) test consisted of 3 phases: familiarization, habituation, and the recognition test, each separated by 24 hours, and were conducted in a manner identical to our previous reports.[17–19] All trials were video recorded and scored offline with The Observer XT software (Noldus, Leesburg, VA) by experimenters blinded to the odor-impregnated bead

(discussed later) and mouse irradiation conditions. Beads and mice were number coded for behavioral scoring of video. One baseline SORM test was completed before surgery and radiation exposure, and the remaining tests occurred at 4-week intervals starting at approximately 2 weeks after the radiation exposure. Different novel social odors from male Long Evans rats housed in a different vivarium were used for each test period. Each familiarization phase started 7 days after the last cage cleaning to provide for distinctive conspecific odor cues. Cages were cleaned after 3 testing phases were completed. The details are described in Supplementary Methods (Appendix E1).

Rodent psychomotor vigilance test—The rodent psychomotor vigilance test (rPVT) is an operant-based attention test that was completed in daily, 30-minute sessions. Mice were first trained to respond on an illuminated nose poke key for food on a fixed ratio 1. Once stable performance was achieved, mice were then trained to respond to illumination of the nose poke key after a variable delay of 3 to 10 seconds. After stable acquisition of the rPVT by achieving at least 75% correct responses during four of five 30-minute sessions per week, mice received surgery for tumor implantation and radiation exposure.

Histology

Mice were anesthetized deeply with isoflurane and perfused intracardially with 5% sucrose followed by 4% paraformaldehyde. Brains were dissected, post-fixed in 4% paraformaldehyde overnight at 4°C, and cryopreserved in 30% sucrose. The brains were cut into 30-μm coronal sections. For Eriochrome cyanine staining, slides were oven-dried and dehydrated in 95% and 70% ethanol. Next, sections were stained with an Eriochrome cyanine solution (0.2% Eriochrome cyanine, 0.4% $FeCl_3$, and 0.5% H_2SO_4). Section development was performed by alternating exposure to 0.1% NH_4OH and rinsing in distilled water until white matter (blue) was clearly differentiated from gray matter. For immunofluorescence staining, the sections were blocked using 0.1% Triton and 5% BSA for 2 hours at room temperature and then incubated overnight with primary antibodies at 4°C. Either Alexa-488 or Alexa-594 (Molecular Probes, 1:200) secondary antibody was added for 2 hours of incubation at a room temperature. Sections were then counterstained with aqueous nonfluorescing mounting (Immu-Mount, Thermo Scientific). The following primary antibodies were used: IBA1 (1:250, Wako); GFAP (1:250, Dako); NeuN (1:100, Cell Signaling Technology). Histochemical and immunofluorescent images were acquired with an inverted microscope (Zeiss, Axio Observer Z1, equipped with ORCA4 camera; Hamamatsu). For quantification of GFAP, IBA1, NeuN, and Eriochrome cyanine staining, entire brain tissue (3–5 brain tissue sections per mouse) images were captured with 10 × magnification and measured with Image J. The value for contralateral hemisphere was used for the internal control. Data are presented as a ratio (intensity or area of ipsilateral or contralateral hemisphere).

Statistical analysis

The histologic and immunofluorescence data are presented as the mean ± standard deviation. The normal distribution was analyzed using the Shapiro-Wilk test. For data normally distributed, a 2-tailed Student *t* test was used when comparing 2 groups. One-way analysis of variance (ANOVA) with Tukey post hoc was used when comparing 3 groups. For data

not normally distributed, Mann-Whitney test was used when comparing 2 groups. Kruskal-Wallis test was used when comparing 3 groups. Survival curves were generated using Kaplan-Meier method and analyzed using the log-rank test. For the SORM test, paired *t* tests were used to compare the exploration of the novel 2 and novel 1 odors on the recognition test for each group; to control for multiple *t* tests, the Holm-Sidak method was used. Separate repeated-measures analysis of variances were used to examine rPVT performance changes for each measure, followed by Dunnett multiple comparison post hoc test, when needed. All statistical analyses were performed using GraphPad Prism 8. A value of $P \leq .05$ was considered statistically significant.

Results

Eradication of brain tumors with SRS

Logarithmic tumor growth was observed with BLI in all grafted animals up to day 9, and it continued in untreated animals until their death at approximately 3 weeks after tumor inoculation (tumor group). In stark contrast, the BLI signal started declining 1 week after SRS, completely disappeared 3 weeks after treatment (Fig. 1C, 1D), and it never recurred within the 18-month observation period in any of the animals (Tumor + SRS group).

MRI was acquired to visualize the brain tissue response to tumor and to SRS, and it complemented results from BLI (Fig. 1E). In the nontreated group, the tumor grew as a bulk without infiltration and compressed the ipsilateral cerebral ventricle and the contralateral hemisphere in the end stage. In the treated group, the tumor initially seemed to increase its volume 1 week after SRS, although its border was less distinct. The clear tumor regression was observed from 2 weeks after SRS onward, with heterogeneous texture including regions of hyperintensity (likely necrosis) and some hypointensities (likely microhemorrhages). Moreover, BLI signal of the tumor cells had decreased to background level 4 weeks after SRS, whereas the tumor region was still visible as a mixture of hypointense and hyperintense spots at week 4 and a hypointense area at week 8 (Fig. 1E, 1F). Kaplan-Meier curve and log-rank tests further confirmed a significant increase in median survival of the tumor + SRS group (no animal was dead at 79 weeks' follow-up) in comparison to the tumor group, in which all animals were deceased by day 30 after tumor implantation ($P < .001$; Fig. 1G). Taken together, the results indicate that the SRS was capable of eradicating the tumor while allowing for long-term survival of all animals.

SRS-induced tumor disintegration and neuroinflammatory response

The tumor core was composed solely of densely packed spindle-shaped tumor cells at 3 weeks after implantation (Fig. E1). In contrast, SRS induced a robust tumor infiltration by microglia/macrophages and changed the morphology and density of tumor cells, now being more multipolar and loosely present (Fig. 1A). No clear influence of SRS on GFAP expression was observed at this time point. No tumor cells were present 10 weeks and 79 weeks after SRS, but both microglia/macrophage activation and astrocytosis were observed at the prior tumor site (Fig. 2C–2F).

SRS-induced cognitive impairment

All animals successfully completed both behavioral tests before and up to 2 weeks after SRS, which proved that the presence of the tumor itself was not a source of cognitive decline (Fig. 3). Starting at 6 weeks after SRS, the tumor + SRS group displayed similar exploration of the novel 2 and novel 1 odors, which illustrates a social recognition memory impairment starting at this time point that continued throughout the remainder of the SORM testing period (Fig. 3A; test 6 at approximately 22 weeks after irradiation). The sham + SRS group did not show social recognition memory impairment until 10 weeks after SRS (Fig. 3C), and this impairment was transient, with significantly greater exploration of the novel 2 odor occurring again at 18 and 22 weeks after SRS (Fig. 3C; $P < .003$). For the rPVT, both groups displayed significantly decreased percent of correct responses and significantly increased attention lapses during the first week of rPVT performance after SRS (ie, at 6 weeks after SRS; Fig. 3B, 3D). However, these changes were similar between the groups and were transient, with both groups showing pre-SRS equivalent performances for the remainder of the testing period (ie, up to 40 weeks after irradiation).

SRS elicited acute and chronic neuroinflammation in the treated area, but not in off-target hippocampus

Neither astrocyte nor microglia/macrophage activation was observed by histology in hippocampus (Fig. E2). These findings have been corroborated with no evidence of asymmetry or signal abnormalities that would indicate edema or inflammation or BBB disruption (Fig. E3). Overall, there was no detectable off-target SRS-induced damage to the hippocampus.

In contrast to the hippocampus, there was pronounced evidence of neuroinflammation (astrocytosis and microglia/macrophage activation) in the targeted area at weeks 2 and 10 after SRS (Fig. 4A, 4B). Quantitative analysis of $GFAP^+$ and $IBA1^+$ staining (ipsilateral/contralateral positive area) revealed that the ipsilateral hemisphere had a significant enhancement in both astrocyte and microglia/macrophage infiltration in all groups of animals subjected to SRS ($P < .001$; Fig. 4C, 4D). In addition, we found that the neuroinflammation level in the tumor + SRS group was significantly greater than in the sham + SRS group at week 2 (Fig. 4C; $P < .001$), but not at week 10 (Fig. 4D; $P > .05$). Furthermore, after the acute stage at week 2, the neuroinflammation at week 10 declined in both groups (Fig. 4A, 4B, quantified in Fig. 4E), except for the $IBA1^+$ microglia/macrophage infiltration area in the sham + SRS group, as there was no significant difference between weeks 2 and 10 (Fig. 4E), which presumably occurred because of the absence of tumor clearance in this group.

High-dose irradiation leads to neither neuronal degeneration nor demyelination in early stage

NeuN and Eriochrome cyanine staining were performed on coronal brain sections from the center of radiation beam at tumor implantation sites to investigate the effect of SRS on neurons and oligodendrocyte function. There was no asymmetry in the Eriochrome cyanine staining at weeks 2 and 10 after irradiation in both groups (Fig. 5A), and there was no significant difference in ipsilateral/contralateral intensity between each group (Fig. 5B). The

mice in the Tumor + SRS group (n = 3) at week 10 after SRS were used for assessment of neuronal degeneration. NeuN staining did not detect asymmetry (Fig. 5C), and there was no significant difference in ipsilateral/contralateral fluorescence intensity between the sham and tumor + SRS groups (Fig. 5D). Thus, the data indicated that the early neurobehavioral impairment was unlikely to be associated with demyelination and neuronal degeneration.

Long-term (79 weeks) follow-up on late radiation-induced brain injury

To identify the long-term consequences of radiation-induced tumor eradication, mice from the tumor + SRS group (n = 3) were monitored using MRI until week 79 after treatment, followed by histologic assessment. In anatomic T2WI, there was no hyperintensity indicative of edema or necrosis at any of the time points, whereas hypointensity appeared at week 10 after treatment, indicative of microhemorrhaging, and some hypointensity remained up to week 79 (Fig. 6A). In addition, there was no evidence of BBB breach at any tested time point, as evidenced by a lack of Gd enhancement on T1WI (Fig. 6A, quantified in Fig. 6B). To further explore the effect of SRS on brain atrophy, the ipsilateral/contralateral hemisphere area was measured at the 4 time points. As shown in Fig. 6C, the SRS-treated (ipsilateral) hemisphere at week 24 started to show a slight volume reduction ($P < .01$), indicating brain atrophy. There was some progression of atrophy, but the difference between weeks 24 and 79 was not statistically significant (Fig. 6C). In behavioral assessment (psychomotor and social memory tests), deficits persisted in tumor-bearing irradiation-treated animals throughout the testing period until week 42 (Fig. 3). As shown in Figure 6D, some degree of neuroinflammation (astrocyte or microglia/macrophage activation) was detected at week 79, whereas neither neuronal degeneration nor demyelination occurred even at that late time (Fig. 6D, 6E).

Discussion

We have shown that brain tumor disintegration resulting from SRS treatment leads to persistent cognitive decline. In contrast, exposure of healthy brain tissue to SRS results in transient cognitive deficits only. Notably, SRS did not affect animal survival in both animal groups until the end of the study at the 18-month time point. Our results are particularly relevant to the ongoing controversy over the selection of optimal radiotherapeutic strategy. In addition, the increasing cure rate of metastatic brain disease has brought more attention to the quality of life and cognitive function of survivors. Therefore, there is observed expansion of indications for SRS application in brain metastasis control over traditional whole brain tumor radiation therapy (WBRT), owing to presumably lower neurotoxicity and better early control of metastases.[3,20] The oligorecurrence can also be safely managed using a noncoplanar, mono-isocenter SRS technique, with impressive 1-year overall survival in 77% of patients.[21] Therefore, the number of patients experiencing favorable outcomes is sufficient to justify the inquiry into their cognitive status and quality of life. In particular, our study reveals that SRS-induced tumor disintegration with subsequent neuroinflammatory response might be a source of cognitive decline, whereas the same dose of SRS applied to healthy brain tissue is behaviorally more benign. Thus, further work on the precision of SRS delivery can actually fail to provide additional cognitive benefits because the impairment might stem from tumor breakdown rather than imprecise irradiation. Notably, one clinical

study confirmed faster cognitive decline in a WBRT + SRS group at 4 months, but it also revealed that an impressive 73% of patients subjected to WBRT + SRS were free from central nervous system (CNS) recurrence in comparison to so few as 27% of patients who received SRS alone.[22] Our preclinical study has shown that radiation-induced cognitive deficits can be transient and that tumor disintegration poses more threat to long-term permanent function. Therefore, we hypothesize that some level of up-front whole brain irradiation preventive of metastasis recurrence might be more beneficial than repeated exposure of the brain to the metastasis disintegration. This hypothesis is in line with a recent clinical trial in which prophylactic cranial irradiation in patients with non-small cell lung cancer (NSCLC) decreased the number of symptomatic brain metastases, while not affecting health-related quality of life.[23] The recent research on predilection of pathologic types of lung cancer to certain brain regions might also open an avenue to a concept of regional brain radiation therapy depending on the primary cancer, which would further limit burden of brain metastatic disease.[24]

Therefore, the larger studies of brain function after SRS for brain metastases are warranted. We postulate that a sudden hit of brain metastasis with SRS could lead to relatively fast tumor disintegration and release of potentially toxic and neuroinflammatory molecules to the surrounding tissue, which in turn potentiate cognitive impairment. Therefore, gentler approaches to tackle metastases or strategies battling neuroinflammation might be preferable. Fractionation of stereotactic radiation dose might spread the tumor disintegration over a longer period of time, which might potentially avoid a sudden exposure of surrounding brain to factors released from decomposing tumor. The molecular approaches and immunotherapies, even if not highly effective, currently might be a forward-looking approach capable of tumor elimination in a temperate fashion.[25–27] The precise, image guided intra-arterial delivery of macro-molecules, such as antibodies to the brain across osmotically open BBB, might be an attractive route to deliver biologics to the brain metastases.[28] There is also progress in the design of small molecules, which may cross BBB, such as third-generation EGFR tyrosine kinase inhibitor osimertinib, which provided encouraging results in early clinical trial in patients with EGFR mutation-positive NSCLC,[29] although enthusiasm to this approach needs to be tempered by the risk of chemobrain occurrence.

Although the comprehensive assessment of cognitive function in patients subjected to SRS is warranted, it is also tempting to use our model to study the effects of both tumor disintegration and various therapeutic approaches on cognitive deficits. The major advantage of our experimental setting is not only tumor eradication, but also persistent cognitive deficits in long-lived animals. The SORM behavioral test is relatively easy to execute in any animal facility, and automation of data processing should facilitate their adaptation by the research community. We hypothesize that the long-lasting cognitive deficits might be related to the neuroinflammatory processes associated with tumor disintegration. Activation of microglia and astrocytes with secretion of proinflammatory factors in response to radiation injury was shown to disrupt cell—cell signaling, cell function, and differentiation in the central nervous system contributing to radiation-induced cognitive dysfunction.[30–34] The activation of microglia/macrophage and astrocytes were observed in response to local radiation and tumor disintegration. As expected, in our

present study we found that microglia/macrophage and astrocyte infiltration were greater in the tumor-bearing brain than in the tumor-free brain after SRS, implicating the role of tumor disintegration in exacerbating neuroinflammation, which is associated with the persisted cognitive dysfunction. The findings indicate that neuroinflammation can be an important target for intervention to prevent or mitigate cognitive dysfunction. Actually, the anti-inflammatory agent (L-158, 809) and elimination of microglia have been demonstrated to improve cognitive function after whole-brain irradiation.[35–37] Recently, in a preclinical study, Feng et al[38,39] showed that transient inhibition of colony-stimulating factor 1 receptor reduced microglia activation after fractionated brain irradiation, resulting in rescue of cognitive function. In addition to pharmacologic interventions, more advanced radiation techniques hold promise for ameliorating the adverse effects of radiation for cancer survivors. It has been shown that FLASH does not induce neurocognitive impairment, and it is associated with less tissue toxicity and reduced neuroinflammation.[4] Another technological advancement is to improve the accuracy of radiation delivery with image guided radiation therapy. Image guided radiation therapy enables better precision and target localization, allowing for reduction of planning margins and a smaller volume of healthy tissue irradiated at high doses.[40] Proton radiation therapy is an emerging approach with a substantial advantage over the conventional radiation therapy because of the unique depth-dose characteristics, which can significantly lower the dose to normal tissue.[41] All the advanced radiation therapy techniques aim to increase the dose in the target tumor and minimize the dose in the surrounding healthy tissue. However, our study cautions that the technological progress could reduce the potential toxicity caused by the therapy itself, but it might be not able to avoid the toxicity to the brain tissue because of the tumor disintegration, which should be taken into account.

It is well established that the hippocampus is critical to memory and cognition.[42] In this study, we observed transient memory impairment in the group, indicating that the spatial specificity of the arc treatment allowing to spare the hippocampus effectively preserves (to most extent but not completely) memory function in the absence of tumor breakdown and related neuroinflammation. Indeed, our laboratory and others have shown that nonhippocampal regions are necessary for the formation of social recognition memories, such as the medial prefrontal cortex[19] and perirhinal cortex, regions that were subject to radiation treatment in the current study. Of note is that only sparing the hippocampus may be an overly simplistic view to attenuate all SRS-induced memory impairment. The same view was also proposed by Greene-Schloesser et al[43] that radiation-induced cognitive impairment likely reflects damage to both hippocampal- and nonhippocampal-dependent domains. In our observations, there were limited changes in the different measures of attention on the rPVT that were found only at weeks 6 or 7 after SRS. However, there were no differences between the groups, and both groups continued to display pre-SRS levels of performance for the remainder of the post-SRS testing period. Taken together, the behavioral assessments suggest that the proposed local radiation here led to transient social recognition memory deficit in naive animals, which resulted in persisted cognitive decline owing to brain metastases disintegration. Other neurobehavioral changes were limited presumably because of the use of the arc radiation treatment and limiting radiation dose to the whole brain.

In addition to neuroinflammation, the direct effect of radiation on main functional neural components—namely, neurons and myelin has to be considered. We assessed these elements in the early stage (2 and 10 weeks) and late (79 weeks) after radiation. Notably, we did not find any neuronal loss or demyelination. A similar conclusion was described in a study by Shi et al,[44] in which they found radiation-induced cognitive impairment in the absence of alteration in the number of mature neurons and structural integrity of myelin.[44] Our longitudinal MRI from the early stage (6 weeks after radiation) to the late stage (1.5 years after irradiation) further validated the histologic observation. There was no indicator of brain necrosis, bleeding, or BBB breakdown, but mild brain atrophy in the treated hemisphere was found starting at week 24 after SRS. In addition, histologic evidence from the animals at 1.5 years (79 weeks) after treatment indicated that neurons and myelin were still preserved, whereas mild neuroinflammation was present, in agreement with an early report showing sustained activation of astrocytes and microglia until the endpoint of that study (6 months after irradiation).[30] Therefore, the observations challenge the dogma that radiation affects precursor cells, although the brain tissue might respond differently to hypofractionation of radiation dose than to SRS, which is delivered in a single session.[45]

Limitations

We report that neuroinflammation after SRS-induced brain tumor disintegration contributes to persistent cognitive decline, but the study is not devoid of limitations. We used costimulatory antibody blockades (CTLA4-Ig and MR-1) to induce immunologic tolerance toward brain tumor xenograft. This points to the risk of increased cross-species inflammatory response against the tumor in comparison to same-species clinical setting. Our published and unpublished data showed full protection of human xenograft tumor cells at least up to 200 days; therefore, we do not expect an exacerbation of neuroinflammatory response in our model. However, the confirmation of our results in a syngeneic model in future studies is warranted.

We found higher levels of $IBA1^+$ microglia/macrophage and astrocytosis after tumor disintegration compared with that in naive irradiated animals, and we interpreted these findings as neuroinflammation. These markers and phenotypes have been reported to be main contributors to cognitive impairment.[36,38] However, more evidence is needed to fully characterize the nature of this process, including analysis of peripheral immune cell infiltration and cytokine assessment in the brain after radiation therapy. Furthermore, cerebral vasculature and particular tumor microvascularization before and after SRS would be important components not analyzed as part of this study, but they are shown to drive immune mediators and cells.[46,47]

The present study used a single dose of 40 Gy SRS rather than a fractionated approach, and the reason for that was the capability of eradicating 9L gliosarcoma with long-term survival of treated animals, thus facilitating studies of the late effects of irradiation in the context of disintegrating brain tumor. This protocol made it possible to observe severe neuroinflammation and persistent neurocognitive decline. Fractionation radiation therapy is a standard strategy for brain tumor treatment, which enables to reduce the potential normal tissue toxicity and inflammation. The effect of fractionated irradiation on tumor growth and

cognitive function was not studied by us. Our study indicates a behavioral risk of rapid tumor disintegration by a single dose SRS, which provides a basis for further studies on blunting neuroinflammatory response by dose fractionation. Overall, dose fractionation was previously justified by a more selective direct radiation effect on tumor cells, and our study could warrant another reason for hypofractionation, such as slower tumor disintegration and a lower risk of permanent cognitive deficits.

Conclusion

Overall, the single-arc 40-Gy radiation we used in the present study eradicated the local 9L brain metastases, resulting in survival benefit in the absence of severe brain injury, although neuroinflammation, early neurobehavioral impairment, and late brain atrophy were observed. In addition, the study revealed that tumor disintegration leads robust neuroinflammation and persistent cognitive decline, and these phenomena were independent of the hippocampus. Although targeting neuroinflammation is a promising strategy to prevent or ameliorate cognitive impairment, more effort has to be made as diminished quality of life is an increasing concern for cancer survivors.

Supplementary Material

Refer to Web version on PubMed Central for supplementary material.

Acknowledgments

This study was supported by 2017-MSCRFF-3942, 2019-MSCRFF-5031, NIHR01NS091110, R01NS102675, R21NS091599, R21NS106436.

References

1. Walczak P, Janowski M. Chemobrain as a product of growing success in chemotherapy - focus on glia as both a victim and a cure. Neuropsychiatry (London) 2019;9:2207–2216. [PubMed: 31316584]
2. Achrol AS, Rennert RC, Anders C, et al. Brain metastases. Nat Rev Dis Primers 2019;5:5. [PubMed: 30655533]
3. Badiyan SN, Regine WF, Mehta M. Stereotactic radiosurgery for treatment of brain metastases. J Oncol Pract 2016;12:703–712. [PubMed: 27511715]
4. Simmons DA, Lartey FM, Schuler E, et al. Reduced cognitive deficits after FLASH irradiation of whole mouse brain are associated with less hippocampal dendritic spine loss and neuroinflammation. Radiother Oncol 2019;139:4–10. [PubMed: 31253467]
5. Verhaak E, Gehring K, Hanssens PEJ, Aaronson NK, Sitskoorn MM. Health-related quality of life in adult patients with brain metastases after stereotactic radiosurgery: a systematic, narrative review. Support Care Cancer 2020;28:473–484. [PubMed: 31792879]
6. Armour M, Ford E, Iordachita I, Wong J. CT guidance is needed to achieve reproducible positioning of the mouse head for repeat precision cranial irradiation. Radiat Res 2010;173:119–123. [PubMed: 20041766]
7. Doblas S, He T, Saunders D, et al. Glioma morphology and tumor-induced vascular alterations revealed in seven rodent glioma models by in vivo magnetic resonance imaging and angiography. J Magn Reson Imaging 2010;32:267–275. [PubMed: 20677250]
8. Shapira-Furman T, Serra R, Gorelick N, et al. Biodegradable wafers releasing Temozolomide and Carmustine for the treatment of brain cancer. J Control Release 2019;295:93–101. [PubMed: 30605703]

9. Bow H, Hwang LS, Schildhaus N, et al. Local delivery of angiogenesis-inhibitor minocycline combined with radiotherapy and oral temozolomide chemotherapy in 9L glioma. J Neurosurg 2014; 120:662–669. [PubMed: 24359008]
10. Khil MS, Kolozsvary A, Apple M, Kim JH. Increased tumor cures using combined radiosurgery and BCNU in the treatment of 9l glioma in the rat brain. Int J Radiat Oncol Biol Phys 2000;47:511–516. [PubMed: 10802380]
11. Semenkow S, Li S, Kahlert UD, et al. An immunocompetent mouse model of human glioblastoma. Oncotarget 2017;8:61072–61082. [PubMed: 28977847]
12. Srinivas NR, Shyu WC, Weiner RS, Tay LK, Greene DS, Barbhaiya RH. Pharmacokinetics of CTLA4Ig (BMS-188667), a novel immunosuppressive agent, following intravenous and subcutaneous administration to mice. J Pharm Sci 1995;84:1488–1489. [PubMed: 8748333]
13. Foy TM, Shepherd DM, Durie FH, Aruffo A, Ledbetter JA, Noelle RJ. In vivo CD40-gp39 interactions are essential for thymus-dependent humoral immunity. II. Prolonged suppression of the humoral immune response by an antibody to the ligand for CD40, gp39. J Exp Med 1993;178:1567–1575. [PubMed: 7693850]
14. Liang Y, Walczak P, Bulte JW. The survival of engrafted neural stem cells within hyaluronic acid hydrogels. Biomaterials 2013;34:5521–5529. [PubMed: 23623429]
15. Ngen EJ, Bar-Shir A, Jablonska A, et al. Imaging the DNA alkylator melphalan by CEST MRI: an advanced approach to theranostics. Mol Pharm 2016;13:3043–3053. [PubMed: 27398883]
16. Guide for the Care and Use of Laboratory Animals. 8th ed. Washington (DC); 2011.
17. Jones CB, Mange A, Granata L, et al. Short and long-term changes in social odor recognition and plasma cytokine levels following oxygen (^{16}O) ion radiation exposure. Int J Mol Sci 2019;20:339.
18. Mange A, Cao Y, Zhang S, et al. Whole-body oxygen (^{16}O) ion-exposure-induced impairments in social odor recognition memory in rats are dose and time dependent. Radiat Res 2018;189:292–299. [PubMed: 29332539]
19. Robinson S, Granata L, Hien RD, et al. Temporary inactivation of the medial prefrontal cortex impairs the formation, but not the retrieval of social odor recognition memory in rats. Neurobiol Learn Mem 2019; 161:115–121. [PubMed: 30953696]
20. O'Beirn M, Benghiat H, Meade S, et al. The expanding role of radiosurgery for brain metastases. Medicines (Basel) 2018;5.
21. Nicosia L, Figlia V, Mazzola R, et al. Repeated stereotactic radiosurgery (SRS) using a non-coplanar mono-isocenter (HyperArc) technique versus upfront whole-brain radiotherapy (WBRT): a matched-pair analysis. Clin Exp Metastasis 2020;37:77–83. [PubMed: 31691873]
22. Chang EL, Wefel JS, Hess KR, et al. Neurocognition in patients with brain metastases treated with radiosurgery or radiosurgery plus whole-brain irradiation: A randomised controlled trial. Lancet Oncol 2009; 10:1037–1044. [PubMed: 19801201]
23. Witlox WJA, Ramaekers BLT, Joore MA, et al. Health-related quality of life after prophylactic cranial irradiation for stage III non-small cell lung cancer patients: Results from the NVALT-11/DLCRG-02 phase III study. Radiother Oncol 2019;144:65–71. [PubMed: 31733490]
24. Wang G, Xu J, Qi Y, Xiu J, Li R, Han M. Distribution of brain metastasis from lung cancer. Cancer Manag Res 2019;11:9331–9338. [PubMed: 31802951]
25. Boire A, Brastianos PK, Garzia L, Valiente M. Brain metastasis. Nat Rev Cancer 2020;20:4–11. [PubMed: 31780784]
26. Han RH, Dunn GP, Chheda MG, Kim AH. The impact of systemic precision medicine and immunotherapy treatments on brain metastases. Oncotarget 2019;10:6739–6753. [PubMed: 31803366]
27. Ascha MS, Wang JF, Kumthekar P, Sloan AE, Kruchko C, Barnholtz-Sloan JS. Bevacizumab for the treatment of non-small cell lung cancer patients with synchronous brain metastases. Sci Rep 2019;9:17792. [PubMed: 31780762]
28. Lesniak WG, Chu C, Jablonska A, et al. A distinct advantage to intraarterial delivery of (89)Zr-Bevacizumab in PET imaging of mice with and without osmotic opening of the blood-brain barrier. J Nucl Med 2019;60:617–622. [PubMed: 30315146]
29. Shetty V, Babu S. Management of CNS metastases in patients with EGFR mutation-positive NSCLC. Indian J Cancer 2019;56: S31–S37. [PubMed: 31793440]

30. Chiang CS, McBride WH, Withers HR. Radiation-induced astrocytic and microglial responses in mouse brain. Radiother Oncol 1993;29: 60–68. [PubMed: 8295989]
31. Hwang SY, Jung JS, Kim TH, et al. Ionizing radiation induces astrocyte gliosis through microglia activation. Neurobiol Dis 2006;21: 457–467. [PubMed: 16202616]
32. Ramanan S, Kooshki M, Zhao W, Hsu FC, Riddle DR, Robbins ME. The PPARalpha agonist fenofibrate preserves hippocampal neurogenesis and inhibits microglial activation after whole-brain irradiation. Int J Radiat Oncol Biol Phys 2009;75:870–877. [PubMed: 19801103]
33. Schindler MK, Forbes ME, Robbins ME, Riddle DR. Aging-dependent changes in the radiation response of the adult rat brain. Int J Radiat Oncol Biol Phys 2008;70:826–834. [PubMed: 18164853]
34. Makale MT, McDonald CR, Hattangadi-Gluth JA, Kesari S. Mechanisms of radiotherapy-associated cognitive disability in patients with brain tumours. Nat Rev Neurol 2017;13:52–64. [PubMed: 27982041]
35. Robbins ME, Payne V, Tommasi E, et al. The AT1 receptor antagonist, L-158,809, prevents or ameliorates fractionated whole-brain irradiation-induced cognitive impairment. Int J Radiat Oncol Biol Phys 2009;73:499–505. [PubMed: 19084353]
36. Acharya MM, Green KN, Allen BD, et al. Elimination of microglia improves cognitive function following cranial irradiation. Sci Rep 2016;6:31545. [PubMed: 27516055]
37. Jenrow KA, Brown SL, Lapanowski K, Naei H, Kolozsvary A, Kim JH. Selective inhibition of microglia-mediated neuroinflammation mitigates radiation-induced cognitive impairment. Radiat Res 2013;179:549–556. [PubMed: 23560629]
38. Feng X, Liu S, Chen D, Rosi S, Gupta N. Rescue of cognitive function following fractionated brain irradiation in a novel preclinical glioma model. Elife 2018;7.
39. Feng X, Jopson TD, Paladini MS, et al. Colony-stimulating factor 1 receptor blockade prevents fractionated whole-brain irradiation-induced memory deficits. J Neuroinflammation 2016;13: 215. [PubMed: 27576527]
40. Franzone P, Fiorentino A, Barra S, et al. Image-guided radiation therapy (IGRT): practical recommendations of Italian Association of Radiation Oncology (AIRO). Radiol Med 2016;121: 958–965. [PubMed: 27601141]
41. Mohan R, Grosshans D. Proton therapy - Present and future. Adv Drug Deliv Rev 2017;109:26–44. [PubMed: 27919760]
42. Lisman J, Buzsaki G, Eichenbaum H, Nadel L, Ranganath C, Redish AD. Viewpoints: How the hippocampus contributes to memory, navigation and cognition. Nat Neurosci 2017;20:1434–1447. [PubMed: 29073641]
43. Greene-Schloesser D, Robbins ME, Peiffer AM, Shaw EG, Wheeler KT, Chan MD. Radiation-induced brain injury: A review. Front Oncol 2012;2:73. [PubMed: 22833841]
44. Shi L, Linville MC, Iversen E, et al. Maintenance of white matter integrity in a rat model of radiation-induced cognitive impairment. J Neurol Sci 2009;285:178–184. [PubMed: 19625028]
45. Monje ML, Mizumatsu S, Fike JR, Palmer TD. Irradiation induces neural precursor-cell dysfunction. Nature Medicine 2002;8: 955–962.
46. Chen CC, Chen YC, Hsiao HY, Chang C, Chern Y. Neurovascular abnormalities in brain disorders: Highlights with angiogenesis and magnetic resonance imaging studies. J Biomed Sci 2013;20:47. [PubMed: 23829868]
47. Corliss BA, Azimi MS, Munson JM, Peirce SM, Murfee WL. Macrophages: An Inflammatory Link Between Angiogenesis and Lymphangiogenesis. Microcirculation 2016;23:95–121. [PubMed: 26614117]

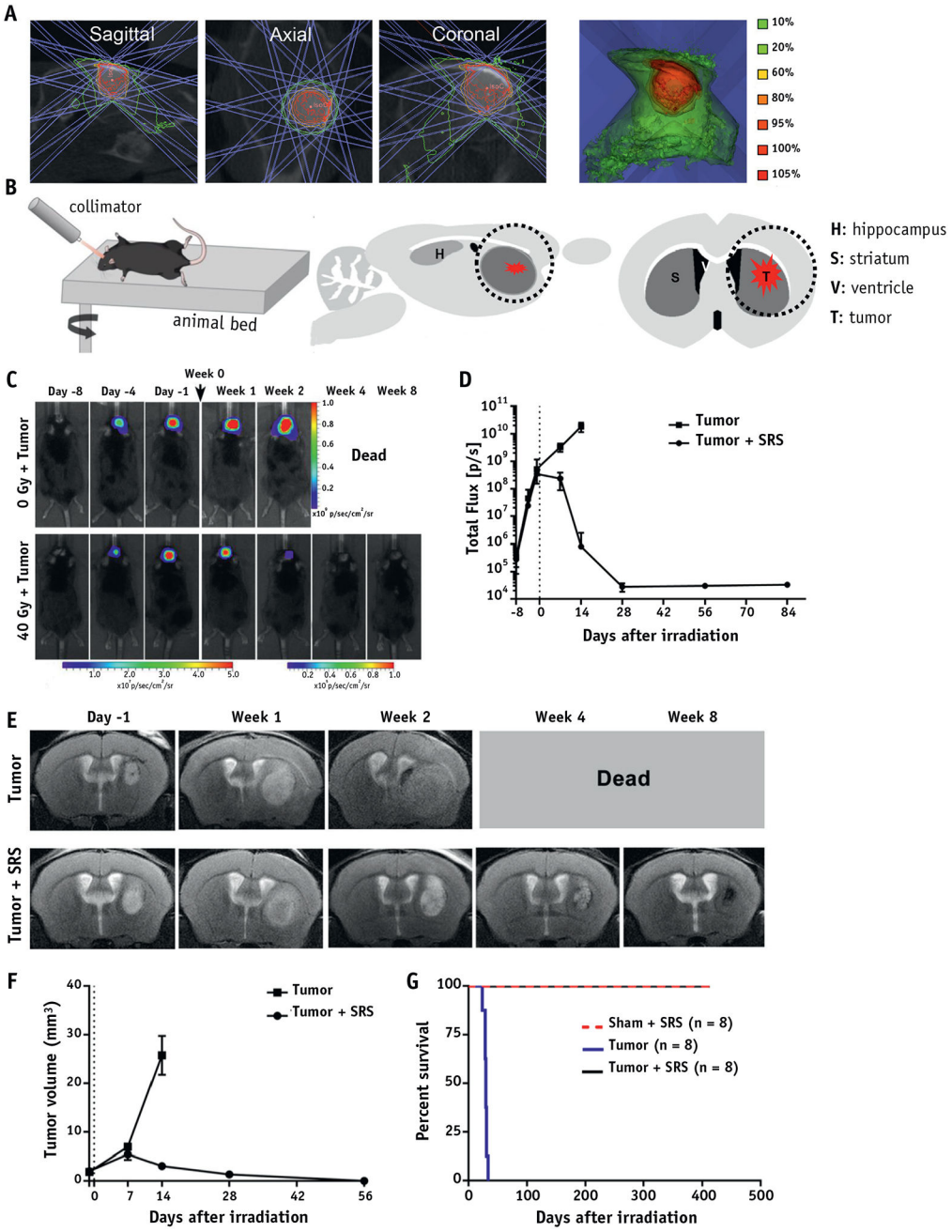

Fig. 1.

Tumor eradication by SRS. (A) Small animal radiation research platform setup shows isodose distribution for 40 Gy using a 5 × 5-mm^2 collimator with a 60-degree arc. (B) The schematic diagram illustrates the SRS treatment and the black circle indicates the involved brain structures. (C) Representative BLI images of non- and SRS-treated tumor-bearing mice at the indicated days (day −1 and week 0 were designated the day before irradiation and the date of irradiation, respectively). (D) Quantification of BLI signal indicated that SRS fully eliminated 9L glioma. (E) Representative T2-weighted MRI images and (F) volumetric analysis of the tumor in non- and SRS-treated tumor-bearing mice, show that the single

dose irradiation of 40 Gy eradicated 9L glioma xenografts. (G) SRS treatment significantly prolonged survival of tumor-bearing mice ($P < .001$), without affecting the survival of naive mice. *Abbreviations:* BLI = bioluminescence imaging; MRI = magnetic resonance imaging; SRS = stereotactic radiosurgery.

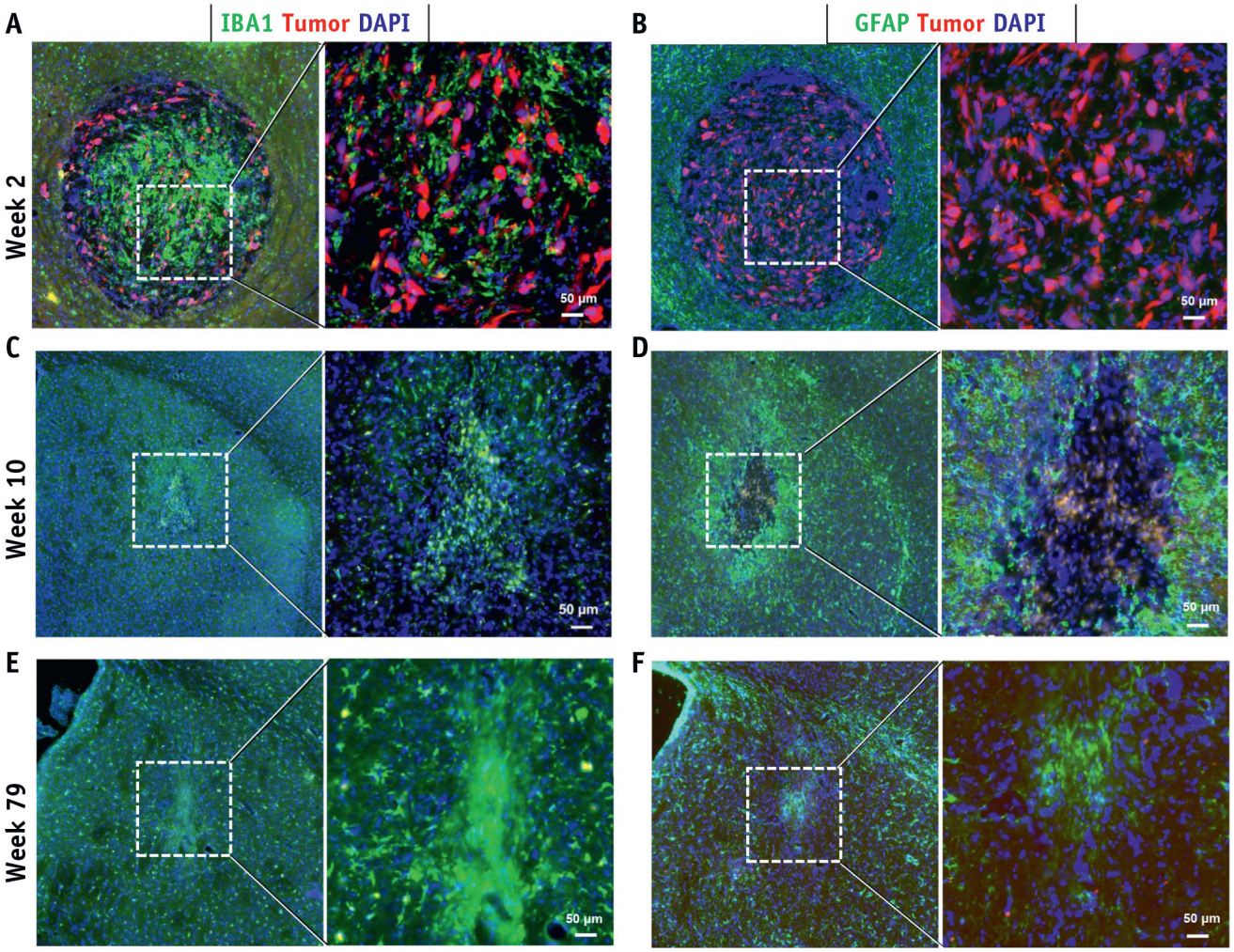

Fig. 2.

Histologic assessment of tumor response to SRS. Tumor cells were visualized by (A-F) fluorescent reporter (*mCherry*; Red) at weeks 2, 10, 79 after SRS. Neuroinflammation inside and surrounding the tumor core was revealed by (A, C, E) $IBA1^+$ microglia/macrophages and (B, D, F) $GFAP^+$ astrocytes. *Abbreviation*: SRS = stereotactic radiosurgery. (A color version of this figure is available at https://doi.org/10.1016/j.ijrobp.2020.05.027.)

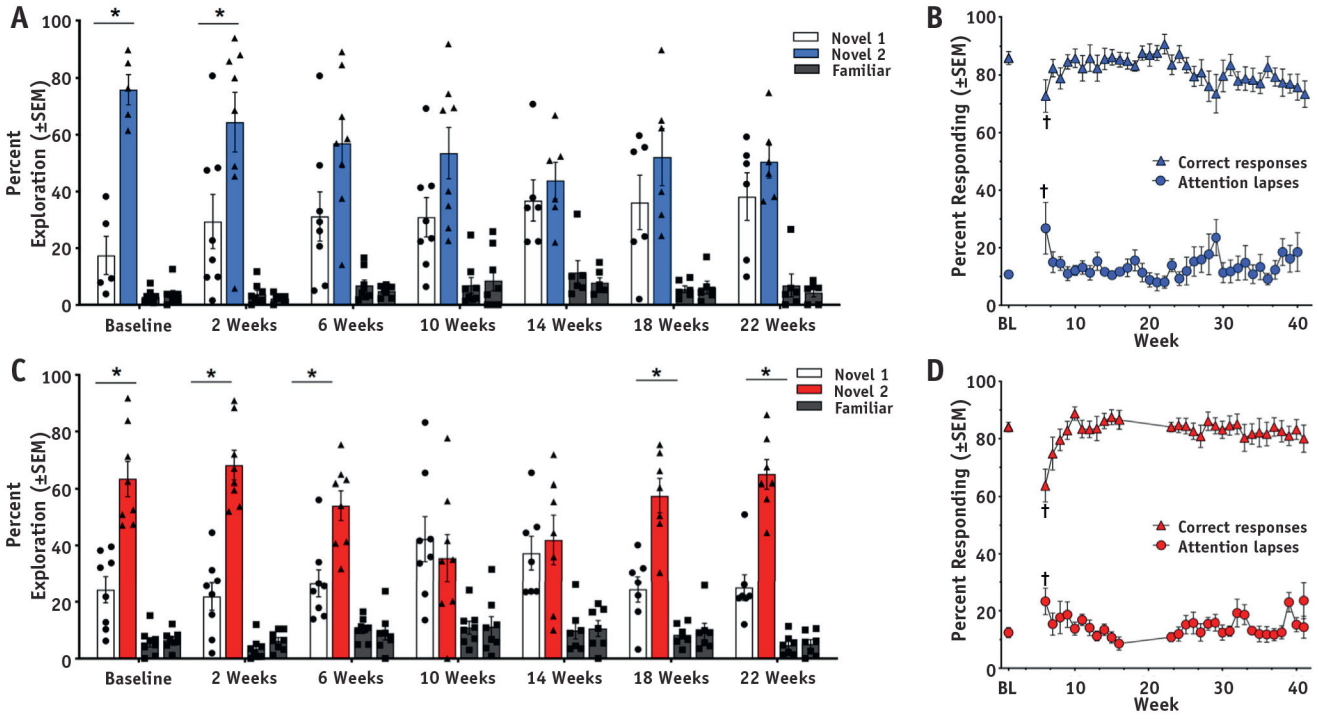

Fig. 3.

Neurobehavioral assessment in animals after SRS. Neurobehavioral performance in the SORM and rPVT in the (A, B) tumor + SRS and (C, D) sham + SRS groups, respectively. $^{*}P < .05$ between the Novel 2 and Novel 1 odor at each SORM test. $^{\dagger}P < .05$ for correct responses and attention lapses on the rPVT.

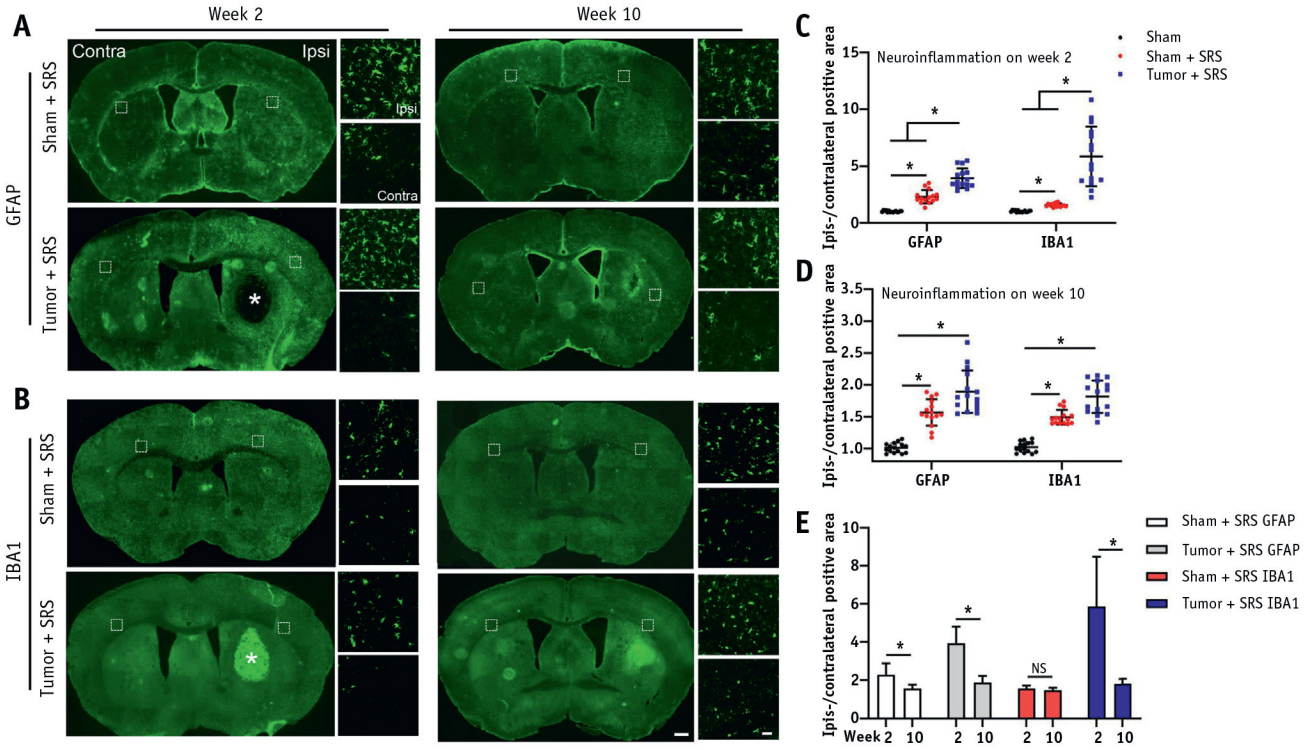

Fig. 4.

Longitudinal assessment of neuroinflammation after SRS. Coronal fluorescent images of mouse brain showed activation of (A) GFAP$^+$ astrocytes and (B) IBA1$^+$ microglia/macrophages at week 2 and 10 after SRS. Quantification of the ipsilateral/contralateral positive area for GFAP and IBA1 between the sham, sham + SRS, and tumor + SRS groups at (C) week 2 and (D) week 10 after irradiation. (E) Quantification of GFAP and IBA1 immunoreactivity and its change between weeks 2 and 10 after SRS in sham + SRS and tumor + SRS groups. The white asterisk indicates the tumor location; n = 3 per group (5 brain tissue sections per mouse). The scale bars for low and high-power images = 500 um and 50 um, respectively; *$P < .01$. *Abbreviations*: NS = no significant difference; SRS = stereotactic radiosurgery.

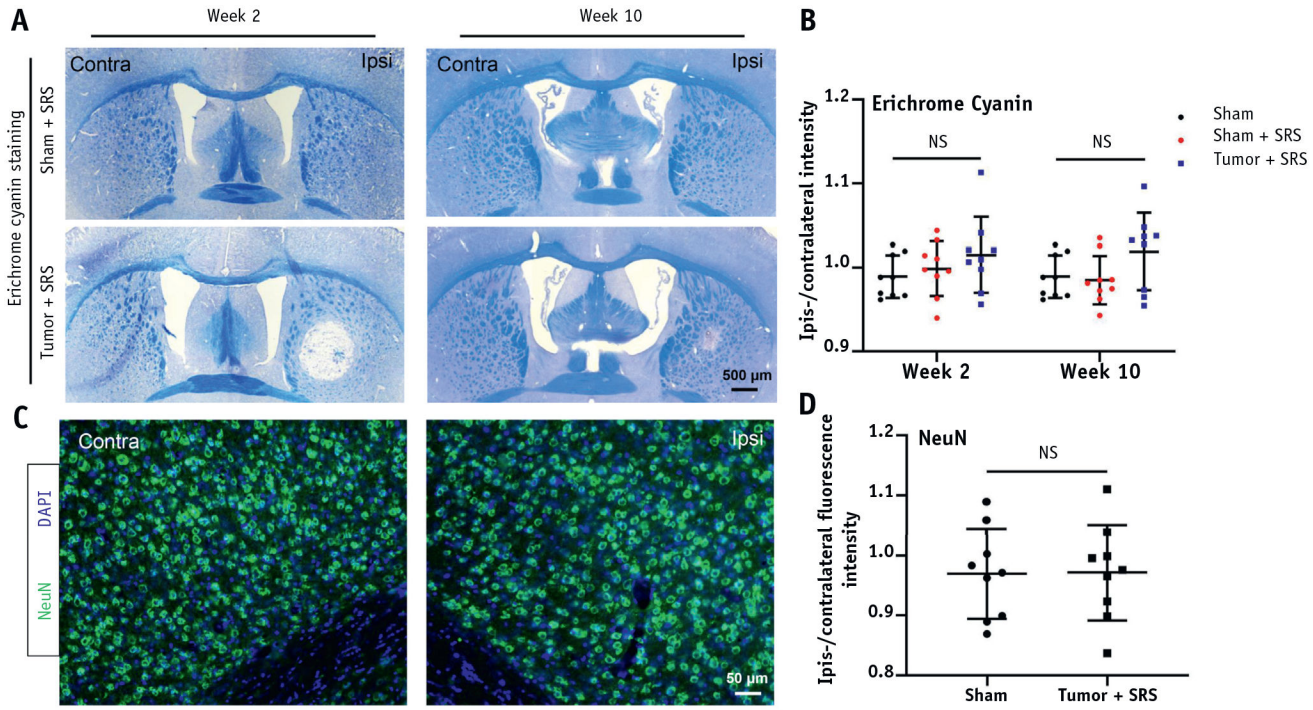

Fig. 5.

Eriochrome cyanine and NeuN staining for assessing myelin and neuronal integrity. (A) Representative images of Eriochrome cyanine staining of mouse brain at weeks 2 and 10 after SRS. (B) Quantitative analysis of the ipsilateral/contralateral intensity of Eriochrome cyanine staining for Sham, sham + SRS, and tumor + SRS groups at week 2 and week 10 time points. (C) Representative images of NeuN fluorescent images of a brain from tumor-bearing mouse at week 10 after SRS. (D) Quantification of the ipsilateral/contralateral NeuN fluorescence intensity for Sham and Tumor + irradiation groups. *Abbreviations*: NS = no significant difference; SRS = stereotactic radisurgery.

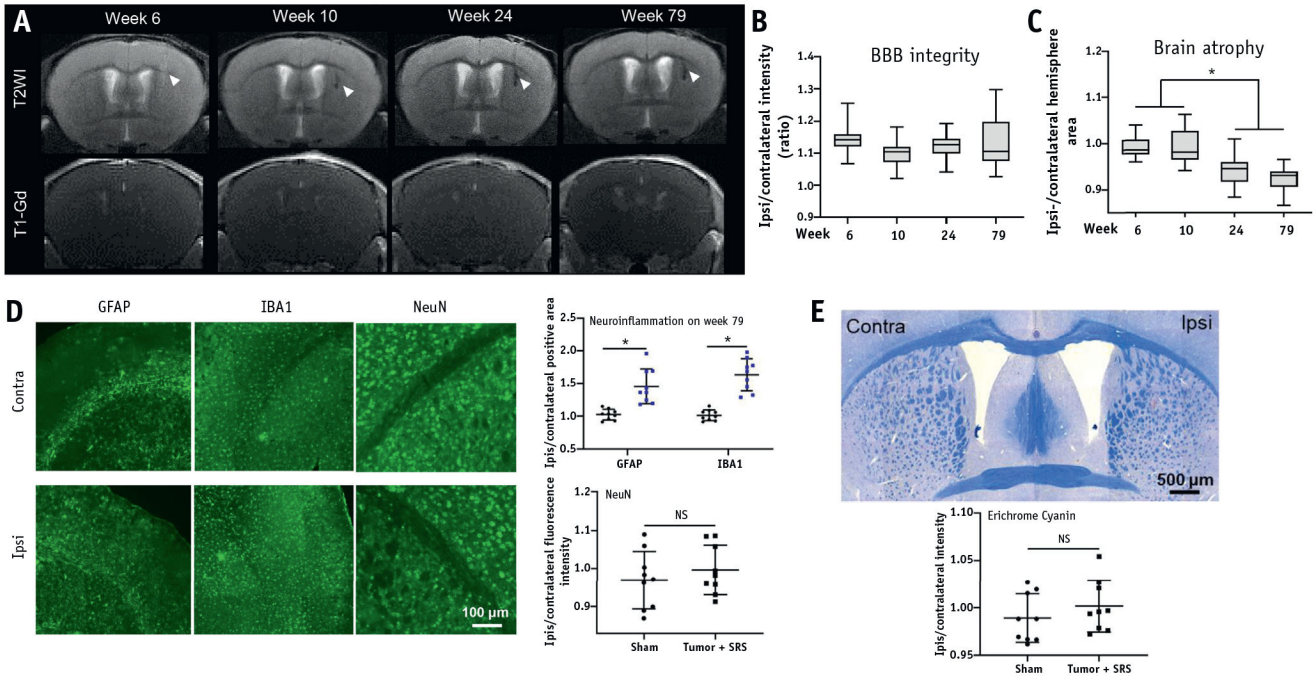

Fig. 6.

Long-term consequences of SRS. (A) Representative images ofT2WI and T1-Gd MRI at weeks 6, 10, 24, and 79 after SRS. (B) Quantitative ipsilateral/contralateral hemisphere intensity based on T1WI. (C) Quantification of ipsilateral/contralateral hemisphere area. (D) Representative images and quantitation of GFAP, IBA1, and NeuN fluorescent staining for neuroinflammation and neuronal damage. (E) Representative image and quantitation of Eriochrome cyanine staining for myelin integrity. White arrowheads points to the necrotic tumor; n = 3 per group (5 brain slices on MRI per mouse, 3 brain tissue sections for histology per mouse). *$P < .01$. *Abbreviations*: MRI = magnetic resonance imaging; NS = no significant difference; SRS = stereotactic radiosurgery; T1WI = T1-weighted imaging; T2WI = T2-weighted imaging.